1D LARGE SIGNAL TIME-DOMAIN CODE FOR TWT

D. T. Lopes[1] and C. C. Motta[2]
[1] Instituto de Pesquisas Energéticas e Nucleares (danieltl@usp.br)
[2] Universidade de São Paulo (ccmotta@usp.br)
São Paulo, SP, Brazil

Abstract

In this paper we describe the development of a 1D large signal code for traveling-wave tubes (TWT) modeling. This code is based in a mathematical model, which extend previous analysis by including the effects of the DC space-charge force in the electron dynamics description in time domain. As a consequence, a previous knowledge of the space-charge reduction factor or its evaluation is no longer needed. As a drawback, this code was shown to be not suitable for multi-drive frequency simulations. Therefore, we compiled a secondary code using the already established theory with an improved space-charge reduction factor, which is function of both the frequency and the modulation signal level. We present a numerical example comparing the results of the two codes to the results from the known theory.

I. INTRODUCTION

Throughout the history of TWTs, several mathematical models were developed to assist in its design. Among the linear models, also called small-signal models, the Pierce model [1] became the more widespread. However, that type of model was unable to predict the saturated output power of a TWT with satisfactory accuracy, since this phenomenon is intrinsically nonlinear. Some years later, Nordsieck [2] developed a nonlinear lagrangian model that was able to predict the saturation of a system consisting of a progressive wave interacting with an electron beam. That model was able to describe the overtaking between the beam particles, which occurs during the bunching process. However, that model did not consider the effects of space charge. This effect was considered later in the Rowe's work [3] and in later works. Giarola presented a multi-frequency model [4] based on the Nordsieck's nonlinear theory. That model allowed to extend the estimation of amplification for signals composed of more tones and intermodulation products.

More recently, Wöhlbier presented a nonlinear eulerian model [5] that could be used for an excitation signal containing an arbitrary number of frequencies without increasing complexity of the model. Additionally, [5] also presented a lagrangian version (LATTE) of that eulerian code (MUSE), since lagrangian codes can better predict the behavior of the TWT near the saturation point.

All the models mentioned here are one-dimensional, i.e., the particles have only axial movement. The electron beam is described as a sequence of disks, whose electric field is obtained by Gauss' law and is weighted by a space charge reduction factor (R_{sc}). The calculation of this factor is by itself a problem of great importance since it significantly affects the physics of the problem. Analytical formulae for calculating the R_{sc} for certain special cases are found in [6]. The code CHRISTINE 1D [7] evaluates the R_{sc} considering a sheath helix around the e-beam.

The above mentioned TWT codes neglect the effects of the DC space charge force by assuming a neutralizer ion background around the e-beam. In the present work, we develop a TWT time domain model computing both the AC and DC space charge forces. This code is suitable for simulating the amplification of a single-frequency drive signal and its harmonics. However, for a multi-drive frequency simulation this code was shown to be impracticable. Therefore, for this purpose, we compiled a code based on the known theory [5] rather using an improved R_{sc} that is calculated by the main code. The referred codes consider $R_{sc}=R_{sc}(\omega)$ as a function of the frequency only. In our analysis, $R_{sc}=R_{sc}(\omega,|V|)$ is a function of the frequency and the signal level, given by the modulating signal voltage amplitude $|V|$.

In next section, we describe the TWT model and the obtaining of the $R_{sc}(\omega,|V|)$. In section III, we present a comparison among the results of the codes for a numerical example available in the literature [5].

II. LARGE SIGNAL MODEL

In this section we describe the development of the time domain TWT code and the obtaining of the space-charge reduction factor.

A. The e-Beam Model

The e-beam is modeled by N_d disks of charge q regularly spaced by dz_0. The e-beam length must be enough to cover the interaction circuit length and the length corresponding to the disks that are going to enter the interaction circuit during the simulation time. Due to the DC space-charge force, the ends of the e-beam will spread out, increasing their velocity on the front end and

This work was supported in part by FAPESP (The State of São Paulo Research Agency) under project 2008/05286-1 and FINEP (Research and Projects Financing) under contract 01.06.0911.01.

978-1-4577-0631-8/12/$26.00 ©2011 IEEE

slowing down at the back end. Therefore, additional e-beam length has to be considered due to this effect in both ends. The key point of the beam discretization and positioning is to keep a constant charge density along the interaction circuit during the whole time simulation when no modulation is present. Fig. 1 shows an illustrative picture of the discretization scheme.

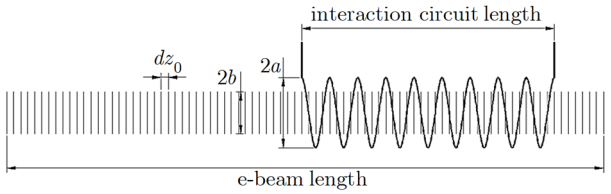

Figure 1. Illustrative scheme of the e-beam discretization along the interaction circuit.

The equation system for the discretized e-beam under DC and AC space charge forces is

$$\begin{aligned} &for\ j \in 1 \ldots N_d \\ &\begin{cases} \dfrac{d}{dt} z_j(t) = u_j(t) \\ \dfrac{d}{dt} u_j(t) = \dfrac{1}{m} \displaystyle\sum_{\substack{i=1 \\ i \neq j}}^{Nd} F_d\left(z_i(t) - z_j(t)\right) + \eta E(z_j(t), t) \end{cases} \end{aligned} \tag{1}$$

The symbols $z_j(t)$ and $u_j(t)$ denote, respectively, the position and the velocity of the *j*-th disk in the time t. The symbol $F_d(\Delta z)$ denotes the DC space-charge force and $E(z,t)$ is the axial electric field in the position z and time *t*. The force $F_d(\Delta z)$ can be evaluated using the following analytic formula

$$F_d(\Delta z) = \frac{\Delta z}{|\Delta z|} \frac{2}{\pi \varepsilon_0} \frac{q^2}{b^2} \sum_{n=1}^{\infty} \frac{J_1^2(x_{0,n} b/a)}{x_{0,n}^2 J_1^2(x_{0,n})} e^{-\frac{x_{0,n}}{a}|\Delta z|} \tag{2}$$

for the cases where the ratio helix radius/beam radius is about 2 or greater. Otherwise, we recommend the use of an electrostatic solver to compute the forces between a pair of disks of charge. In this case, an actual tape or wire helix around the e-beam can be taken into account, resulting in a more accurate force function.

The electric field is evaluated by solving the interaction circuit equation system, as it is described in the next section.

B. Interaction Circuit Model

The TWT interaction circuit is modeled by one or more sections of transmission lines, as illustrated in Fig. 2. In Fig. 2, $V(z,t)$ and $I(z,t)$ are, respectively, the RF voltage and the RF current along the transmission line, $R(z,t)$ is the surface resistivity of the interaction circuit, and $G(z,t)$ is the conductance responsible for the power loss in the helix dielectric supports. We describe the capacitance and inductance distributed along the transmission line in terms of its interaction impedance $K_0(z,\omega)$ and its phase velocity $u_p(z,\omega)$.

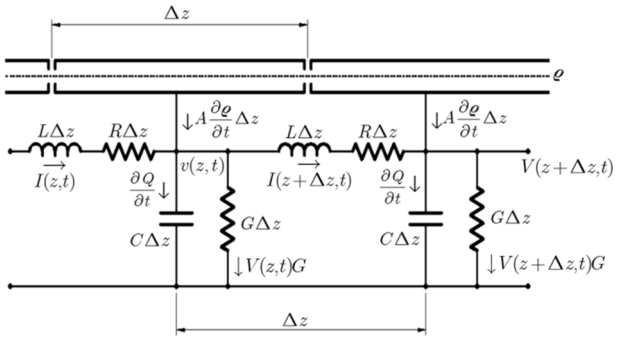

Figure 2. Distributed parameters model for a transmission line coupled to an electron beam.

Developing the equations for voltage and current transmission line, we have the very well-known telegrapher equation system.

By hypothesis, the signals to be amplified are periodic in time with the fundamental angular frequency ω_0 and the fundamental period $T=2\pi/\omega_0$. Therefore, expanding the voltage, the current, and the charge density in Fourier series, the system of equations in the continuous frequency becomes discrete in N_f frequencies, i.e.

$$\begin{aligned} &for\ n = 1 : N_f \\ &\begin{cases} \dfrac{d}{dz} V_{1,n}(z) = -R_n(z) I_{1,n}(z) - \dfrac{\omega_n K_{0,n}(z)}{u_{p,n}(z)} I_{2,n}(z) \\ \dfrac{d}{dz} V_{2,n}(z) = -R_n(z) I_{2,n}(z) + \dfrac{\omega_n K_{0,n}(z)}{u_{p,n}(z)} I_{1,n}(z) \\ \dfrac{d}{dz} I_{1,n}(z) = -G_n(z) V_{1,n}(z) - \dfrac{\omega_n V_{2,n}(z)}{u_{p,n}(z) K_{0,n}(z)} + A\omega_n \rho_{2,n}(z) \\ \dfrac{d}{dz} I_{2,n}(z) = -G_n(z) V_{2,n}(z) + \dfrac{\omega_n V_{1,n}(z)}{u_{p,n}(z) K_{0,n}(z)} - A\omega_n \rho_{1,n}(z) \end{cases} \end{aligned} \tag{3}$$

The parameters R, G, K_0, and u_p are obtained via cold models for the interaction circuit or by means of measurement. The indexes 1 and 2 denote respectively the even and odd expansion coefficients of the Fourier series. The coefficients $\rho_{1,n}(z)$ and $\rho_{2,n}(z)$ represent the harmonic charge density components of the Fourier series. We obtain the charge density term from the solution of the particle dynamics.

C. Beam-Circuit Coupling

The coupling between the equation system for the e-beam dynamics (1) and the equation system for the solution of the RF voltage and current in the interaction circuit (3) is illustrated in Fig. 3.

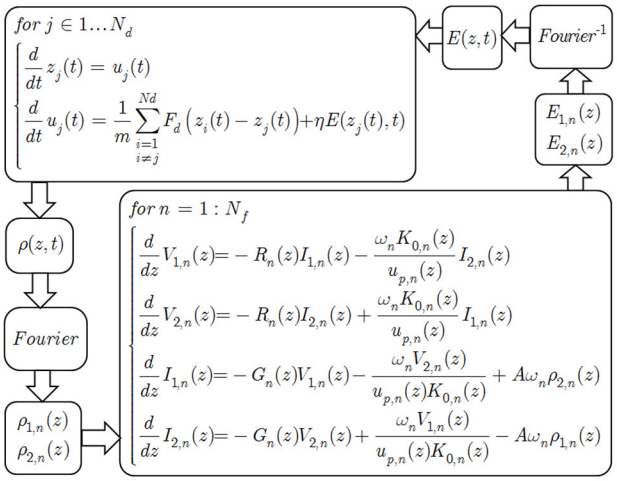

Figure 3. Flowchart of the coupling scheme between the equation systems for the beam dynamics and for the interaction circuit.

From the solution of the charged particles dynamics, we obtain the charge density. Using the Fourier series expansion, we obtain the coefficients of the harmonic charge density. These coefficients are the source terms in the solution of the equation of the transmission line. Solving the transmission line, we obtain the distribution of harmonic current, harmonic voltage and harmonic electric field along the transmission line. Using the inverse Fourier transformation, we rebuild the time varying electric field to be used in the next step in the solution of the particles dynamics equation system (1).

We calculate the charge density by means of the relative shift of particles, which initially were equally spaced, indicating a uniform initial charge density along the interaction circuit. Because of the velocity modulation performed by the axial electric field associated with the excitation signal, the particles have their relative positions changed, implying in a variation of charge density. The charge density at a given position of the circuit at the instant of interaction is given by

$$\rho(z,t) = \rho_0 \left| \frac{\partial z_0}{\partial z(z_0,t)} \right|, \tag{4}$$

where $z(z_0,t)$ is the position of a given particle in terms of its initial position and the instant of time.

Performing the Fourier series expansion, the harmonic charge density coefficients are given by

$$\rho_{1,n}(z) = \frac{2\rho_0 u_0}{N_d/\lambda_0} \sum_{j=1}^{N_d/\lambda_0} \frac{\cos(\omega_n t_j(z))}{u_j(z)}, \tag{5}$$

$$\rho_{2,n}(z) = \frac{2\rho_0 u_0}{N_d/\lambda_0} \sum_{j=1}^{N_d/\lambda_0} \frac{\sin(\omega_n t_j(z))}{u_j(z)}. \tag{6}$$

It is not necessary to take more than one group of samples given by N_d/λ_0, because when the system reaches the steady state, the information from other groups of samples ($2N_d/\lambda_0, 3N_d/\lambda_0$,...) is redundant.

After solving the equation system (3) for each frequency component, the time varying electric field along the interaction circuit may be rebuild from the Fourier coefficients

$$E(z,t) = \sum_{n=1}^{N_f} \left\{ \left[R_n(z) I_{1,n}(z) + \frac{\omega_n K_{0,n}(z)}{u_{p,n}(z)} I_{2,n}(z) \right] \cos(\omega_n t) + \left[R_n(z) I_{2,n}(z) - \frac{\omega_n K_{0,n}(z)}{u_{p,n}(z)} I_{1,n}(z) \right] \sin(\omega_n t) \right\}, \tag{7}$$

which contributes to the AC part of the space charge force in the next iteration of the equation system (1).

D. The multi-frequency simulation

In this type of model for TWT, the way to simulate a multi-frequency amplification is to assume a baseband frequency from which all signals (carriers, harmonics and intermodulation products) are multiples. Thus, the index n in (4) assumes only values that correspond to the frequencies of interest. The code based on (1) and (4) worked as expected for amplification of a carrier and its harmonics. However, for a practical case with two carriers it was shown to be impracticable. As the carriers are spectrally close, the baseband frequency decreases. For cases of interest, the baseband wavelength is about a hundred times the length of the interaction circuit. This implies a beam length of the same order, making the solution infeasible due to the huge number of disks required for the simulation. Additionally, the simulation time required to achieve convergence makes this approach impractical.

The solution for the simulation of the amplification of several carriers was to write a code based on the known theory [5]. This secondary code is built entirely in the frequency domain, and ignores the DC space charge force. However, we compute an enhanced space charge reduction factor $R_{sc} = R_{sc}(\omega, |V|)$, which is a function of both the frequency and the modulating signal level.

E. The Space Charge Reduction Factor

There are some formulas in the literature to calculate the R_{sc}, but they involve approximations in the slow-wave structure. Usually, the structure around the beam is considered as a metallic pipe [6], which is a good approximation when the ratio helix radius over beam radius is 2 or greater. A more elaborated formula [7] considers a sheath helix around the electron beam.

On the other hand, the space charge reduction factor can be "measured" from the interference pattern of space charge waves generated in the electron beam by the disturbance caused by the modulating signal [8]. Using the code based on the equation systems (1) and (3), we can simulate the excitation of space charge waves and analyze their interference pattern. As a result of the

interference of these waves, we see peaks and valleys in the harmonic charge density curve. The position of the first peak corresponds to $\lambda_q/4$ in the case of a klystron type modulation and to $\lambda_q/2$ in the TWT case. The symbol λ_q denotes the reduced plasma wavelength. Using a DC space-charge force calculated by an electrostatic solver for an actual slow-wave structure, it is possible to find accurate space-charge reduction factors. A more detailed description of this work can be found in [9].

Moreover, this analysis allowed us to consider the effect of the modulator signal amplitude. It is known that, at the end of the interaction circuit, the electric field associated with traveling waves has sufficient amplitude to promote overtaking among the electrons. As an effect, the reduced plasma wavelength is decreased, which points an increased in the space-charge reduction factor.

III. NUMERICAL EXAMPLE

In this numerical example, the TWT is modeled by a single section with the parameters shown in Table I and Table II of [5]. The results presented below were obtained using the three variants of the code developed. Namely: TD denotes the variant in the time domain, considering the DC space-charge force. This is the main code of this work. The code in the frequency domain in which the space-charge reduction factor is a function only of the frequency is denoted by $FD-R_{sc}(f)$, which represents the known theory [5]. Last, $FD-R_{sc}(f,|V|)$, denote the code in the frequency domain where the space-charge reduction factor is a function of both the frequency and the level of the modulating signal, which is our solution for the problem of multi-frequency simulation.

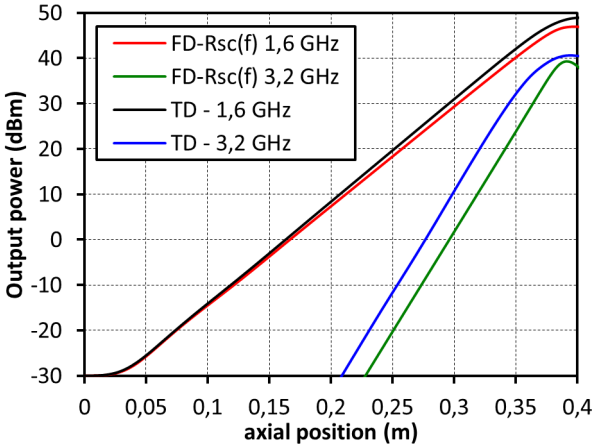

Figure 4. Output power (in dBm) as a function of the axial position along the interaction circuit.

Figure 4 shows the amplification of a drive signal at 1.6 GHz and its first harmonic at 3.2 GHz in order to compare the codes TD and $FD-R_{sc}(f)$. For the drive signal, the power predicted by TD grows up to 2 dB more than the power predicted by $FD-R_{sc}(f)$ at saturation. For the harmonic signal, TD predicts a power 8 dB higher than $FD-R_{sc}(f)$ in the small signal region. At saturation, this difference is reduced to 1 dB.

Figure 5 presents the phase space of electrons along the interaction circuit. We note that the phase space of the electron beam is smoother when the effect of DC space charge force is not considered. On the other hand, when we consider the DC space charge force, the electronic bunches also "push" the electrons just ahead, thus preventing their sudden loss of kinetic energy. This could

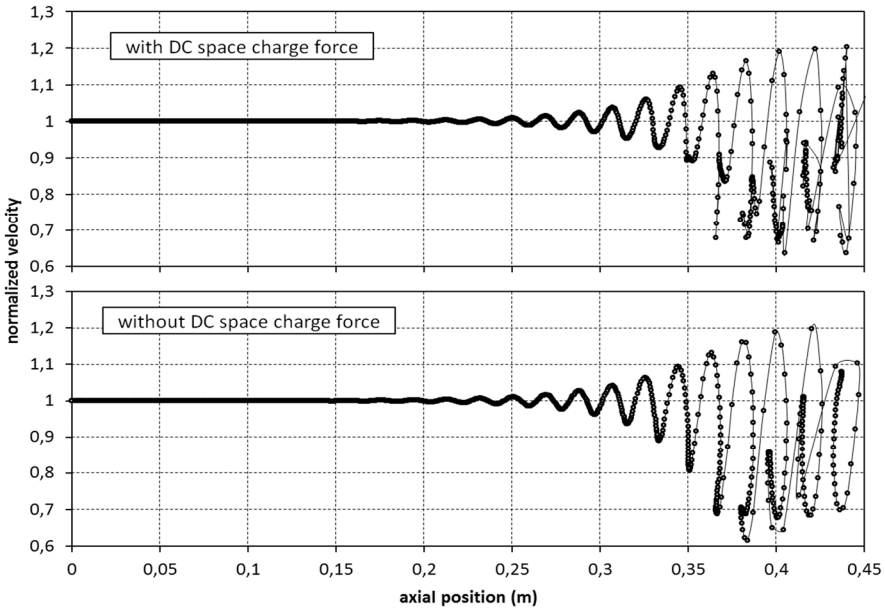

Figura 5. Electron beam phase space for the numerical example simulated considering (above) and neglecting (below) DC space charge forces.

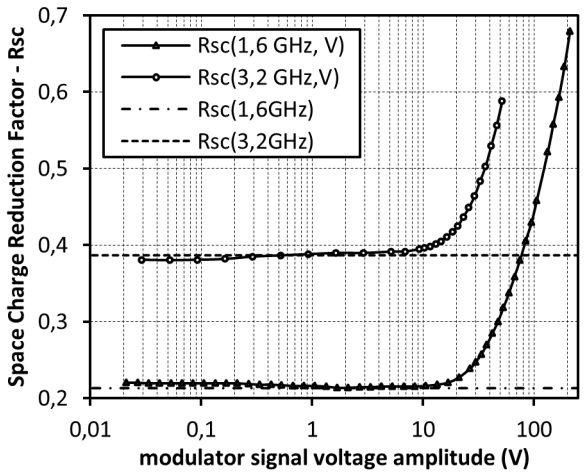

Figure 6. Space charge reduction factor as a function of the modulating signal level for two frequencies.

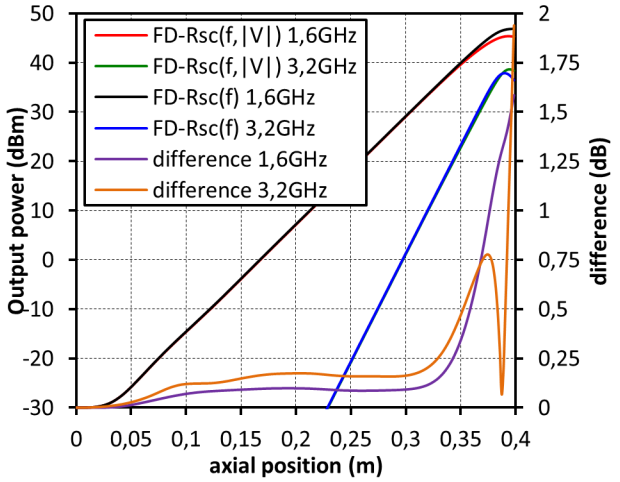

Figure 7. Output power as a function of the axial position predicted by the codes in the frequency domain for the drive signal at 1.6 GHz and its first harmonic.

explain the smoother approach to saturation seen in TD result for the output power. A similar behavior will be seen in the result of the $FD-R_{sc}(f,|V|)$ code.

Figure 6 presents the variation of the space-charge reduction factor for the frequencies of 1.6 GHz and 3.2 GHz as a function of the amplitude of the modulating signal voltage. We note that R_{sc} remain around a fixed value (Table II of [5], which gives $R_{sc}^2(f)$) only during the small signal regime. In the large-signal regime, R_{sc} start to grow up. This variation is due to the variation in the DC space charge forces in the electron bunches.

Figure 7 shows a comparison between the codes $FD-R_{sc}(f,|V|)$ and $FD-R_{sc}(f)$ using the output power as a function of axial position for the 1.6 GHz drive signal and its first harmonic. The difference between the two approaches appears close to the saturation, because of the variation in the space charge reduction factor. As it was observed in the TD result, the $FD-R_{sc}(f,|V|)$ predicts a smoother approach to the saturation. However, in this case, the output power is about 1.5 dB lower. Therefore, the increase of the space charge reduction factor near the saturation is responsible by the smoother approach to saturation observed in the codes TD and $FD-R_{sc}(f,|V|)$.

Figure 8 presents the transfer function, together with the gain curves and AM-AM conversion for the three code variants. The small signal gain predicted by TD is about 2 dB greater than that predicted by the variants in the frequency domain. The 1 dB gain compression point is advanced about 1.5 dB in the $FD-R_{sc}(f)$ result if compared to the other two variants. The AM-AM conversion predicted by TD and by $FD-R_{sc}(f,|V|)$ is in close agreement until -33 dBm. After this point there is divergence, which will be subject of further investigation.

In order to verify the multi-frequency behavior of the

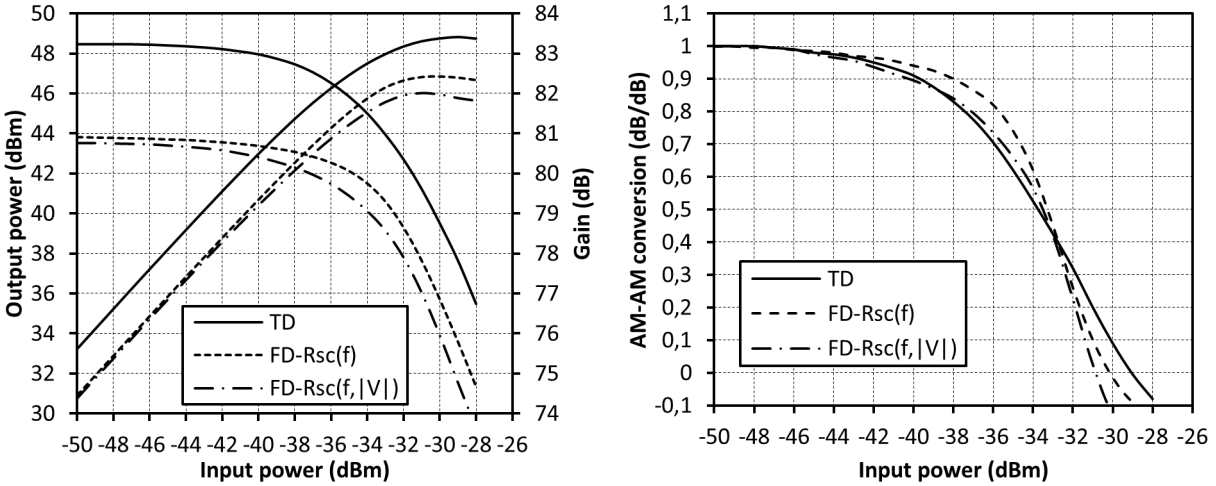

Figura 8. Transfer function and gain (left) and AM-AM conversion (right) predicted by the three codes used in the numerical example simulation.

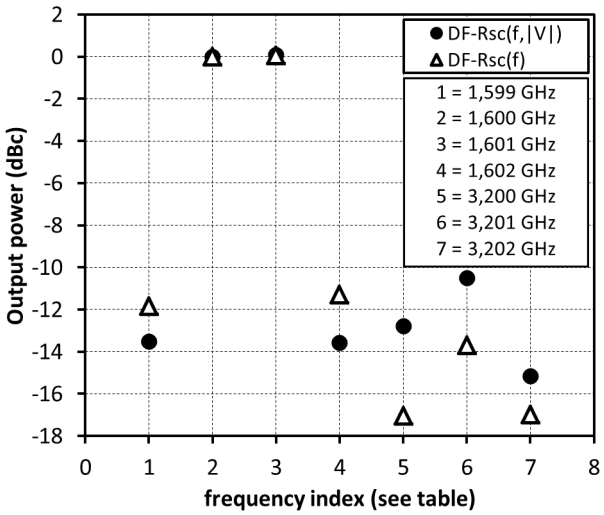

Figura 9. Output power spectrum (in dBc) showing the simulated drive signals, its harmonics and intermodulation products.

code $FD-R_{sc}(f,|V|)$, we simulated the amplification of two tones, 1.600 GHz and 1.601 GHz, its third-order intermodulation products (3IM) at 1.599 GHz and 1.602 GHz and its harmonics 3.2 GHz and 3.202 GHz. The frequency 3.201 GHz was added for convenience. In Fig. 9, we compare the results from $FD-R_{sc}(f,|V|)$ to the ones from $FD-R_{sc}(f)$. Because of its wideband behavior, the characteristics of the simulated TWT section vary less than 1% from 1.599 to 1.602 GHz and from 3.2 to 3.202 GHz. Therefore, we considered the function $R_{sc}(1.6\,GHz,|V|)$ valid from 1.599 to 1.602 GHz. Similarly, we considered $R_{sc}(3.2\,GHz,|V|)$ valid from 3.2 to 3.202 GHz. The carriers are the frequencies indexed by 2 and 3, while the 3IM frequencies are indexed by 1 and 4. The harmonic frequencies are indexed by 5 and 7. The outputs were taken considering a gain compression of 1 dB, as it is usual in the characterization of power amplifiers. The code $FD-R_{sc}(f)$ predicts 3IMs with amplitudes of -11.5 to -12 dB below the carriers, while the code $FD-R_{sc}(f,|V|)$ predicts values about -13.5 dB. The code $FD-R_{sc}(f,|V|)$ also predicts greater amplitude for the harmonics compared to $FD-R_{sc}(f)$. Is must be due to the DC space-charge forces, which prevent smoother overtakes and generates more peaks in the beam current. This effect contributes for a greater harmonic generation.

IV. CONCLUSION

We described the development of codes to simulate the electromagnetic behavior of TWTs and presented a numerical example, whose input data were obtained in the literature. In summary we tested three codes: The code denoted by $FD-R_{sc}(f)$ is our implementation of a theory available in the literature for a multi-frequency code for TWTs. This version does not consider the DC space-charge forces and the space-charge reduction factor is a function of frequency only. The code denoted by TD is our main contribution in his work. This code runs in the time domain and considers the DC space-charge forces. The third code, denoted by $FD-R_{sc}(f,|V|)$ is our solution for multi-frequency simulation. This code considers a space-charge reduction factor that is function of the frequency and the level of the modulating signal as well.

The numerical example presented served to show the level of agreement between the results of our model against those of the model available in the literature. The agreement verified was about 98% for the gain, 96% for the output power. The difference could be explained in the most cases by the effects of the DC space-charge force that we included in our code. Experimental validation is under arrangement.

V. REFERENCES

[1] J. R. Pierce, *Traveling-Wave Tubes*, D. Van Nostrand Company, Inc., New York, 1950.

[2] A. Nordsieck, "Theory of the large-signal behavior of traveling-wave amplifiers," Proc. IRE, vol. 41, pp. 630-637, May 1953.

[3] J. E. Rowe, "A large signal analysis of the traveling-wave amplifier: theory and general results," *IRE Trans. Electron Devices*, vol. 3, pp. 39-57, 1956.

[4] A. J. Giarola, "A theoretical description for the multiple-signal operation of a TWT," *IEEE Trans. Electron Devices*, vol. ED-15, pp. 381–395, June 1968.

[5] J. G. Wöhlbier, J. Booske and Ian Dobson,"The multifrequency spectral eulerian (MUSE) model of a traveling-wave tube," *IEEE Trans. Plasma Sci.*, vol 30, No 3, June 2002.

[6] G.M.Branch and T. G. Mihran."Plasma frequency reduction factors in electron beams," *IRE Trans. Electron Dev.*, April, 1955.

[7] T. M. Antonsen Jr. and B. Levush, "Traveling-wave tube devices with nonlinear dielectric elements," *IEEE Trans. Plasma Sci*., vol. 26, no. 3, pp. 774–786, 1998.

[8] A. S. Gilmour, *Principle of traveling wave tubes*, Artech House, 1994.

[9] D. T. Lopes and C. C. Motta, "Comparison of plasma frequency reduction factors simulated via 1D time domain lagrangian code and expressions in the literature," in Proc. IVEC2011, 2011, p. 131.